RSC Advances

ROYAL SOCIETY OF CHEMISTRY

www.rsc.org/advances

Investigation of Structure and Photocatalytic Activity on TiO_2 Hybridized with graphene：Compared to CNT Case

ShuaiNan Guo, JinChen Fan*, QunJie Xu†, YuLin Min‡

(Shanghai Key Laboratory of Materials Protection and Advanced Materials in Electric Power, College of Environmental and Chemical Engineering, Shanghai University of Electric Power, 200090)

Abstract: The structures of TiO_2 hybridized with graphene by three different methods, i.e., thermal reaction, hydrolyzing synthesis and sol-gel method were studied, and their corresponding photocatalytic activities was compared by degrading Rh.B under UV and visible light irradiation. It was found that the 2-D graphene endowed an excellent morphology and structure for TiO_2 hybridization using arbitrary synthesis routes, providing well-dispersed TiO_2 particles on the graphene sheets with intimate contact. Their photocatalytic Rh.B degradation was strongly dependent on original TiO_2 properties. However, the TiO_2 hybridized with CNT via aforementioned three methods has been determined that their photocatalytic activity was strongly influenced by interfacial structures.

1. introducation

Several strategies have been proposed to increase the efficiency of TiO_2 photocatalyst, among them, the preparation of TiO_2-based composites is an efficient means to enhance the photocatalytic performance via retarding the charge recombination [1]. The composite of TiO_2 and carbon materials, particularly carbon nanotubes (CNTs), has attracted much attention in past two decades [2]. It is proposed that the photogenerated electrons in the space-charge regions may be transferred into CNTs, and the holes remain on TiO_2, thus retarding the recombination of electrons and holes [3]. However, the TiO_2 hybridized with CNTs described a much more sophisticated system in which the hydrophobic and inert nature

*Corresponding Author: JinChen Fan(Email: jinchen.fan@gmail.com);

† Corresponding Author: QunJie Xu(Email:xuqunjie@shiep.edu.cn);

‡Corresponding Author: YuLin Min(Email:ahaqmylin@126.com)

of the CNTs is unfavorable for these applications. For example, Yao et al. have demonstrated that a hydration/dehydration process creating CNT/TiO_2 composites enhanced the photocatalytic activity for degradation of phenol in the liquid phase in comparison to commercial P25 [4]. But the multi-walled carbon nanotube (MWCNT)/TiO_2 composite prepared by this way shows lower photocatalytic activity for degradation of phenol than that over commercial P25. Yu and co-workers reported that a simple mechanical mixture of TiO_2 (P25) and MWCNTs improved the photocatalytic activity of TiO_2 for color removal in an aqueous solution of azo-dyes under UV light [5]. However, the researchers did not fully explain how a simple mixture of TiO_2 and CNTs would interact to accelerate the degradation of the dye.

Most recently, the TiO_2 hybridized with graphene in catalysis field are attempting to draw the fact that graphene can compete with CNTs in charge transfer and separation. Yet the TiO_2 hybridized with graphene system were competing arguments held by exposed some literatures. Dai and co-workers reported that a TiO_2–RGO composite prepared by growing TiO_2 nanocrystals on GO through hydrolysis followed by hydrothermal treatment efficiently catalyzed the photocatalytic degradation of rhodamine B (Rh.B), and there existed strong visible light activity due to possible formation of Ti–O–C bonds [6]. Xiong et al. demonstrated that the RGO–TiO_2 composite with high visible-photocatalytic performance for degradation of Rh.B could be only ascribed to photosensitization process, rather than the excitation of RGO–TiO_2 [7]. Li and co-workers demonstrated that the TiO_2 (P25)–RGO composite was a highly efficient photocatalyst for the degradation of methylene blue (MB) than TiO_2 (P25)–CNTs composite [8]. However, a very recent study by Xu and co-workers pointed out that the TiO_2–RGO composite was in essence the same as the TiO_2–CNTs composite on enhancement of photocatalytic performance in the degradation of MB and methyl orange (MO), and gas-phase degradation of benzene [9]. The remarkable enhancement in the visible light absorption and the photocatalysis of TiO_2 after being hybridized with CNT or graphene is true, but does not make a decision for the photocatalytic process. Therefore, it would be an interesting and important research direction to understanding what affect the photocatalytic activity of TiO_2 by means of CNTs or graphene hybridization.

In this work, we have compared the structure dependent photocatalytic actives of

graphene/TiO_2 and CNTs/TiO_2 using three different synthesis methods, and demonstrated the role contributions between interfacial structures and synthesis routes.

2. Experimental

2.1 Materials

Graphite powder (purity 99.9995%) was obtained from Alpha Aesar. Titanium (Ⅳ) isopropoxide (TIP) and Titanium tetrachloride ($TiCl_4$) were purchased from Aldrich. Sodium nitrate was obtained from Sigma Aldrich, Potassium permanganate from Yakuri chemicals Japan, P25 from the Degussa Company. The hydrogen peroxide and ethanol were obtained from Junsei chemicals, Japan; hydrochloric acid from LT Baker, USA; Rhodamine B (Rh.B) and nitric acid from Daejung Chemical & Metals Co., Ltd., (Korean).

2.2 Synthesis procedure

2.2.1 Synthesis of Graphene Oxide (GO).

GO was prepared from graphite powder according to the modified method reported by Hummers and Offeman. The as-prepared GO was reduced to graphene by using hydrazine hydrate.

2.2.2 Synthesis of graphene/TiO_2 Composites

Graphene/TiO_2 composites were synthesized by three different methods, ie., thermal reaction, hydrolyzing synthesis and sol-gel method, and final products are named as GT-T, GT-H and GT-S, respectively.

Thermal reaction. Graphene was first dispersed in EtOH by ultrasonic treatment for 1 h. Then, P25 was added into the graphene suspension. The suspension was stirred and maintained at 393K for 6h. The resultant product was collected by centrifugation, washed repeatedly with water, and dried in vacuum at 333 K. GT-T composite was finally obtained by heat treatment at 693K for 2h in Ar. CNT/TiO_2 composites was obtained by similar procedure and named as CT-T.

Hydrolyzing synthesis. Graphene was first dispersed in EtOH by ultrasonic treatment for 1 h. Then, $TiCl_4$ was added into the graphene suspension. The suspension was stirred and maintained at 393K for 12h. Meanwhile, $TiCl_4$ was hydrolyzed by adding 5 mL H_2O. The resultant product was collected by centrifugation, washed repeatedly with water, and dried in

vacuum at 333 K. GT-H composite was finally obtained by heat treatment at 693K for 2h in Ar. CNT/TiO_2 composites was obtained by similar procedure and named as CT-H.

Sol-gel method. Graphene was first dispersed in EtOH by ultrasonic treatment for 1 h. Then, TIP was added into the graphene suspension, and 2 mL HNO_3 was added simultaneously. The suspension was stirred and maintained at 393K for 12h. The resultant xerogel was collected by centrifugation, washed repeatedly with water, and dried in vacuum at 333 K. GT-H composite was finally obtained by heat treatment at 693K for 2h in Ar. CNT/TiO_2 composites was obtained by similar procedure and named as CT-S.

2.3 Analysis instruments

XRD patterns were obtained with a diffractometer on Riguka, Japan, RINT 2500 V using Cu Kα radiation. Raman spectra were carried out by a Horiba Jobin Yvon LabRAM using a 100×objective lens with a 532 nm laser excitation. Fourier transform-infrared (FT-IR) spectra were recorded in KBr pellets with Bruker FTIR. Diffuse reflectance UV-visible absorption spectra were obtained using a spectrophotometer (Shimadzu UV-2401PC) equipped with a diffuse reflectance accessory, and $BaSO_4$ was used as the reference. Transmission electron microscopy (TEM) observations were obtained using a JEM-2200FS microscope with Cs correction.

2.4 Photocatalytic activity

In order to analyze the photocatalytic effects, the decomposition reaction of Rh.B in water was followed. Powdered samples of 0.05 g were dispersed in the Rh.B solution under ultrasonicate for 3 min. Before irradiation, the mixture was magnetically stirred for 1 h in the dark to establish adsorption−desorption equilibrium of the dye with the catalyst. For irradiation system, the visible light (λ>420 nm) was used at the distance of 100 mm from the solution in darkness box. The suspension was irradiated with light source as a function of irradiation time. Samples were then withdrawn regularly from the reactor and removal of dispersed powders through centrifuge. The clean transparent solution was analyzed by UV/vis spectroscopy (S-3100, Sainco. Co. Ltd.,). The concentration of Rh.B in the solution was determined as a function of irradiation time from the absorbance region at a UV wavelength line of 550 nm.

Results and discussion

3.1 Photocatalytic activity

Fig. 1a and b show the degradation efficiencies of Rh.B over the GT composites with 5% graphene content prepared by different approaches under UV and visible light irradiation, respectively. For comparison, the results obtained for TiO_2 alone and the CT composites with 5% CNT content prepared by three different methods are also listed in Fig 1a and b. The controlled blank reaction in the absence of any catalyst or in the presence of Gr or CNT alone shows no degradation of Rh.B. The P25 alone shows higher photocatalytic activity than T-H and T-S both under UV and visible light, but T-S processes highest vis-response, the phenomenon will be discussed later. However, the TiO_2 hybridized with graphene composites by all the three methods exhibit significantly enhanced degradation efficiencies of Rh.B than each TiO_2 alone, clearly demonstrating that the presence of graphene can enhance the photocatalytic performance of each TiO_2 for degradation of Rh.B. The order of photocatalytic activities of GT is consistent with that of original TiO_2, suggesting that the photocatalytic activities of GT is mainly influenced by activities of initial TiO_2. Compared with the CT composites, the distinct difference between the two composites in our case suggests that the TiO_2 hybridized with graphene is more suitable for photocatalytic reactions even in use of all the three methods, the results similar to H_2 evolution reactions [10]. However, the CT composite by sol-gel method shows highest photocatalytic activity among three CT composites under both UV and visible light irradiation.

We further investigate the effect of graphene content on photocatalytic activities of GT-T and GT-S under UV and visible light, respectively. As shown in Fig. 1b and c, it is obvious that the GT-T with 5 wt.% graphene and GT-S with 7 wt.% graphene display the highest photocatalytic activity under visible light and UV respectively. It is slightly different compared with that reported by Zhu et al, who used a similar method for preparing graphene/TiO_2 [11]. But the photocatalytic efficiencies of Rh.B over GT-T with different graphene content reveal same trends, namely, first increasing and then decreasing. In GT-S case, a higher content of graphene (7%) in GT-S is required for obtaining the optimum photocatalytic activity under visible light. This may indicate that the graphene acts different

roles in each reaction system. According to above results, sol-gel method seems to be an efficient approach for higher visible response TiO_2, we further compared the photocatalytic activities of CT-S and GT-S with different nanocarbon content. As shown in Fig. S1, the graphene provided a superior photocatalytic activities of Rh.B degradation to CT-S under visible light, indicating that graphene is a more promising candidate for modification of TiO_2.

3.2. Characterizations of GT Composites

Fig. 2 (a-e) shows the high resolution C 1s XPS spectra for the GT composites as well as GO and Gr. In the C 1s spectra, main peaks located at 284.6, 285.6, 286.7, 287.7 and 288.4 eV observed from the C1s deconvolution spectrum of GO correspond to the C–C, C–OH, C–O, C=O, and O–C=O (–COO–) groups, respectively [12]. Compared with GO, the intensity of the C–O peak in graphene together with GT-S and GT-H is decreased significantly, indicating the reduction of GO to graphene sheets and presence of Gr in GT-S and GT-H. Additional component at 283.7 eV corresponding to Ti–C [13, 14] and a raising C–OH at 285.6 eV appear in C1s XPS spectra of GT-S. The observation of the Ti–C signal in the deconvoluted XPS spectrum of the GT-S can be attributed to formation of Ti–C bond between the TiO_2 coating and the disorders of the graphene and/or between the TiO_2 coating and the amorphous carbon [15]. The improvement in the visible light photocatalytic activity of the GT-S corresponding to GT-S and GT-H can be related to formation of Ti–C bond between the graphene and TiO_2 by a sol-gel method. Earlier reports combined theoretic and experiment indicated that the reduction of remaining C–OH groups of GO is very difficult [16, 17]. Titanium alkoxide (Titanium (Ⅳ) isopropoxide in this study) can be readily grafted on the reduced graphene surfaces by chemisorptions at the molecular level; sonication and stirring in succession assist dispersion of the titanium alkoxide among the graphene suspension and promotes the reaction between the titanium precursor and the –OH groups on the graphene surfaces. The GT colloids are formed via hydrolysis reaction between the adsorbed alkoxide and water molecules. The presented HNO_3 act as charger in starring solution, which can render the GT colloids positively charged due to supplying hydroxyl groups by hydrolysis of alkoxide. After sol-gel process finish, the TiO_2 particle can be closely coated on Gr surface, combining this with the XPS results (Figure 2e), we deduce that the Ti–C bond is caused between Gr and TiO_2 at their interface. Generally, Ti^{3+} can also be

created in TiO_2 through the doping of other elements such as C, N, or F species to form the partially reduced product of TiO_{2-x} [18]. In above XPS discussion, it was proven that there is Ti–C bond in GT-S, which means that if the carbon doping occurred in GT-S, and the Ti^{3+} might be detected. Herein, we provided the Ti2p XPS of GT-T, GT-S and GT-H in Fig. S2, where no obvious peaks associated with Ti^{3+} at 456.6 eV could be detected. The results indicate that the Ti–C bond is caused between Gr and TiO_2 at their interface due to surface chemisorptions at the molecular level.

Fig. 2f shows Raman spectra of GT, the peaks around ~144, ~399, ~513, and ~639 cm^{-1} ascribed to anatase TiO_2 [19]. A slight difference of peaks width can be seen among the three GT composites. The energy bonds of the anatase phase are perturbed by the hydrolyzing synthesis and sol-gel methods, which suggests some substitutions of the Ti^{4+} by carbon atoms forming (Ti–O–C or Ti–C) bonds in the TiO_2 lattice. Insert displays that the intensity ratio of D band to G band of graphite, which is gradually enhanced from graphite to graphene, originating from defects associated with vacancies, grain boundaries, and amorphous carbon [20]. Above results are further confirmed by XRD and FT-IR studies (Fig. S3, ESI). In the case of the GT composites, the major peaks for GT-H and GT-S presented in all the diffractograms correspond to the single anatase form of TiO_2. The most widely studied Degussa P25, which at 80% anatase and 20% rutile is also detected in GT-T, produces novel electronic states at anatase–rutile junctions that result in enhanced charge carrier separation, reduced electron–hole recombination, and facilitated charge transfer to adsorbed species [21, 22]. This is an essential why P25 alone and GT-T have higher photocatalytic activity.

More recently, previous studies have demonstrated the enhanced photo-oxidative degradation of organic dyes for both CNT-based and graphene-based TiO_2 nanocomposites [23-25]. In particular, since these photo-oxidative reactions occur primarily on the unmodified TiO_2 surface, few discernible differences have been reported between nanocomposites based on different carbon polymorphs [9]. The TEM images are further complicated by the fact that the higher nanocarbons exhibited multiple isomeric forms with shapes ranging a wall tube for CNT and planar sheets for graphene as shown in Fig. 3. The TEM images of the GT composites show that the composites are composed of graphene sheets and TiO_2 nanoparticles with different size range. The size of these TiO_2 nanoparticles in GT-T, GT-H and GT-S are

~20 nm, ~5 nm and ~7 nm, respectively, and the results are confirmed by their HR-TEM. However, the contact between TiO_2 and graphene is different for the composites prepared by different methods. In the GT-S, TiO_2 nanoparticles are more highly dispersed on graphene sheets, whereas the segregation of TiO_2 nanoparticles from graphene sheets or the aggregation of TiO_2 nanoparticles is serious in the GT-T or GT-H. However, these different morphologies for GT composites are not consistent with their photocatalytic activity. The higher photocatalytic activity of GT-S is attributed to the extended optical absorption, resulting from surface impurity doping (Ti-C bonds). Moreover, the similar morphologies are also found in CT composites. Due to dispersed TiO_2 on CNT surface in dense, the CT-S shows higher photocatalytic activity under both UV and visible light irradiation, which is attributed to the increased lifetimes of the TiO_2 confined holes, due to the injection of photoexcited electrons into the CNT [26]. These TEM measurements further reveal an easy controlling photocatalytic activity of TiO_2 hybridized with CNT, rather, the TiO_2 hybridized with graphene may make a tunable photocatalytic activity.

Diffuse reflectance UV-vis spectroscopy was applied to further study the interaction between TiO_2 and graphene in the composites prepared by three different methods, which are shown in Fig. 4. All GT composites show a red shift of the absorption edge compared to pure TiO_2, suggesting that the carbon may exist in TiO_2 matrix. However, the considerable red shift for GT-S relate to form Ti-C bonds due to in present of C-Ti interfacial structure by attching titanium alkoxide onto functionalized graphene sheets by chemisorption. Therefore, photocatalytic activity of TiO_2 hybridized with graphene can be tuned by various synthesis routes. According to adsorption edge, the T-S has a markedly higher visible absorption tailing down to more than 420 nm due to carbon dopant, which has been confirmed by Choi work [27].

In summary, the photocatalystic activity of TiO_2 hybridized with CNT strongly depend on their structure, a high degree dispersion of TiO_2 on CNT surface by a sol-gel route processes the highest photocatalytic activity for degradation of Rh.B under both UV and visible light irradiation than use of thermal reaction and hydrolyzing synthesis routes, although pure P25 alone shows higher photocatalytic activity. However, the photocatalystic activity of TiO_2 hybridized with graphene is not evidence on dependent of their structure. As

shown in TEM and HR-TEM images, the GT composites prepared by three different methods also show greater distribution features, supporting the creation of an interphase interaction between TiO_2 and graphene. Fig. 5a displays the photographs of the GT suspensions obtained by three different methods. The suspensions of GT are the similar homogeneous dispersion, suggesting a strong interaction between the two components in GT composites. Moreover, the gradual darkening color from CT-T to CT-S can be explained that more impurities as the amorphous carbon is introduced in CT-S, which is related to use of different Ti precursor. The absorption intensity changes in the UV and visible regions over CT composites by three different methods indicate that the chemical reducing graphene as in accordance with the UV-vis spectrum of plain graphene, which are shown in Fig 5b.

Therefore, we deduce that the defect of graphene is major driving force for ideal distributing state of TiO_2 (as shown in Raman data), the defect of graphene with dangling bonds on the basal plane expand their application in different method. As we known in graphene/TiO_2 field, the synthesis approaches include photoreduction method [28], hydrothermal method [29], sol-gel method [30], hydrazine reduction method [11], ionic liquid method [31], molecule graft method [32], water-phase method [33], sonochemical method [34], electrochemical deposition method [35] and liquid phase deposition method [36]. Accelerating distribution of TiO_2 on graphene surface is mainly ascribed to physisorption, electrostatic binding, or through charge transfer interactions. However, some especial properties or morphologies can be observed using different synthesis methods, such as a liquid phase deposition method can form morphology of TiO_2 nanoparticles distributed on the both sides of the graphene sheets [37]. A self-assembly method can construct p/n heterojunction between TiO_2 and graphene interface [38]. In this work, we not only provides an example of graphene/TiO_2 composites using three different method and demonstrated that graphene is a very promising candidate for regulation of photocatalytic activity of TiO_2, but also opens new possibilities to provide some insight into the design of graphene based photocatalysts with high photocatalytic activity in further applications.

4. Conclusion

We have prepared graphene/TiO_2 composites by three different methods, i.e., thermal reaction, hydrolyzing synthesis and sol-gel methods. These composites have shown better

photocatalytic performances for degradation of Rh.B than each original TiO_2 alone. The photocatalytic activity of these composites has strictly arranged in photocatalytic activity order of original TiO_2 under both UV and visible light irradiation, suggesting that the photocatalytic activity of graphene/TiO_2 composites can be tuned by modifying original TiO_2. However, the CNT/TiO_2 composites have shown best photocatalytic performance for degradation of Rh.B by sol-gel route under both UV and visible light irradiation, suggesting that the photocatalytic activity of graphene/TiO_2 composites can be controlled by synthesis method. By investigation of structures of graphene/TiO_2 and CNT/TiO_2 composites, the structures of CNT/TiO_2 composites may cause difference of their photocatalytic activity due to interphase interaction between TiO_2 and CNT, however, the intimate contact between TiO_2 and graphene can be observed by three different methods, which weakens the influence of the transfer of photogenerated electrons.

Acknowledgement

This work was supported by the National Science Foundation of China (NSFC) (Grants nos.21271010) and Shanghai Municipal Education Commission (No:15ZZ088) and Science and Technology Commission of Shanghai Municipality.(No: 14DZ2261000).

References

[1] K. Rajeshwar, N. R. de Tacconi, C. R. Chenthamarakshan, Chem. Mater. 2001, 13, 2765–2782

[2] K. Woan, G. Pyrgiotakis, W. Sigmund, Adv. Mater. 2009, 21, 2233–2239.

[3] M.R. Hoffman, S.T. Martin, W. Choi, W. Bahnemann, Chem. Rev. 95 (1995) 69 – 96

[4] Y. Yao, G. Li, S. Ciston, R.M. Lueptow, K.A. Gray, Environ. Sci. Technol. 42 (2008) 4952–4957.

[5] Y. Yu, J. C. Yu, C.Y. Chan, Y.K. Che, J.C. Zhao, L. Ding, W.K. Ge, P.K. Wong, Appl. Catal., B: Environ. 61 (2005) 1–11.

[6] Y. Liang, H. Wang, H. S. Casalongue, Z. Chen, H. Dai, Nano Res. 2010, 3, 701–705.

[7] J.T. Zhang, Z.G. Xiong, X. S. Zhao, J. Mater. Chem. 2011, 21, 3634-3640

[8] H. Zhang, X. Lv, Y. Li, Y. Wang, J. Li, ACS Nano 2010, 4, 380–386.

[9] Y. Zhang, Z. R. Tang, X. Fu, Y. J. Xu, ACS Nano 2010, 4, 7303–7314.

[10] W. Q. Fan, Q. H. Lai, Q. H. Zhang, Y. Wang, J. Phys. Chem. C 2011, 115, 10694–10701

[11] Y.J. Wang, R. Shi, J. Lin, Y.F. Zhu, Appl. atal.B: Environ. 100 (2010) 179-183

[12] Zhou, Y.; Bao, Q.; Tang, L. A. L.; Zhong, Y.; Loh, K. P. Chem. Mater. 2009, 21, 2950–2956.

[13] Huang Y, Ho W, Lee S, Zhang L, Li G, Jimmy JC. Langmuir 2008;24:3510–6.

[14] H. Sun, Y. Bai, Y. Cheng, W. Jin, N. Xu, Ind. Eng. Chem. Res. 2006;45:4971–6.

[15] O. Akhavan, M. Abdolahad, Y. Abdi, S. Mohajerzadeh, Carbon 47 (2009) 3280–3287.

[16] Boukhvalov D, Katsnelson M. Phys Rev B 2008;78(8):1–5

[17] D.X. Yang, A. Velamakanni, G. Bozoklu, S.J. Park, M. Stoller, R.D. Piner, S. Stankovich, I. Jung, D. A. Field, C. A. Ventrice Jr., R. S. Ruoff, Carbon 47 (2009) 145-152.

[18] J. Zhang, Z. Xiong, X. S. Zhao, J. Mater. Chem. 2011, 21, 3634−3640.

[19] C. Chen, W.M. Cai, M.C. Long, B.X. Zhou, Y.H. Wu, D.Y. Wu, Y.J. Feng, ACS Nano 4 (2010) 6425.

[20] Zhou, Y.; Bao, Q.; Tang, L. A. L.; Zhong, Y.; Loh, K. P. Chem. Mater. 2009, 21, 2950–2956.

[21] A. L. Linsebigler, G. Lu, J. T. Yates, Chem. Rev. 1995, 95, 735–758.

[22] D. C. Hurum, A. G. Agrios, K. A. Gray, T. Rajh, M. C. Thurnauer, J. Phys. Chem. B 2003, 107, 4545–4549.

[23] Y. Yao, G. Li, S. Ciston, R. M. Lueptow, K. A. Gray, Environ. Sci. Technol. 2008, 42, 4952–4957.

[24] K. Woan, G. Pyrgiotakis, W. Sigmund, Adv. Mater. 2009, 21, 2233–2239.

[25] Y. H.Ng, I. V. Lightcap, K. Goodwin, M. Matsumura, P. V. Kamat, J. Phys. Chem. Lett. 2010, 1, 2222–2227.

[26] K. Zhang, F. J. Zhang, M. L. Chen, W. C. Oh, Ultrasonics Sonochemistry 18 (2011) 765–772.

[27] Y.S. Park, W.Y. Kim, H.W. Park, T. Tachikawa, T. Majima, W.Y. Choi, Appl. Catal. B: Environ. 91 (2009) 355–361.

[28] G. Williams, B. Seger, P. V. Kamat, ACS Nano 2008, 2, 1487–1491.

[29] F. Wang, K, Zhang, J. Mol. Catal. A: Chem. 345 (2011) 101–107

[30] Zhang, X. Y.; Li, H. P.; Cui, X. L.; Lin, Y. J. Mater. Chem. 2010, 20, 2801–2806.

[31] J.F. Shen, M. Shi, B. Yan, H.W. Ma, N. Li, and M.X. Ye, Nano Res. 4, (2011), 795-806

[32] Y.B. Tang, C.S. Lee, J. Xu, Z.T. Liu, Z.H. Chen, Z.B. He,Y.L. Cao, G.D. Yuan, H.S. Song, L.M. Chen, L.B. Luo, H.M. Cheng, W.J. Zhang, I. Bello, S.T. Lee, ACS Nano 4 (2010) 3482–3488.

[33] C.Z. Zhu, S.J. Guo, P. Wang, L. Xing, Y.X. Fang, Y.M. Zhai, S.J. Dong, Chem. Commun, 2010, 46, 7148–7150.

[34] J.J. Guo, S.M. Zhu, Z.X. Chen, Y. Li, Z.Y. Yu, Q.L. Liu, J.B. Li, C.L. Feng, D. Zhang, Ultrason.Sonochem. 18 (2011) 1082–1090.

[35] N.L. Yang, J. Zhai, D. Wang, Y.S. Chen, L. Jiang, ACS Nano. 4 (2010) 887–894.

[36] H.J. Zhang, P.P. Xu, G.D. Du, Z.W. Chen, K. Oh, D.Y. Pan, Z. Jiao, Nano Res 4 (2011) 274–283.

[37] G.D. Jiang, Z.F. Lin, C. Chen, L.H. Zhu, Q. Chang, N. Wang, W. Wei, H.Q. Tang, Carbon. 49 (2011) 2693–2701.

[38] C. Chen, W.M. Cai, M.C. Long, B.X. Zhou, Y.H. Wu, D.Y. Wu, Y.J. Feng, ACS Nano. 4 (2010) 6425–6432.

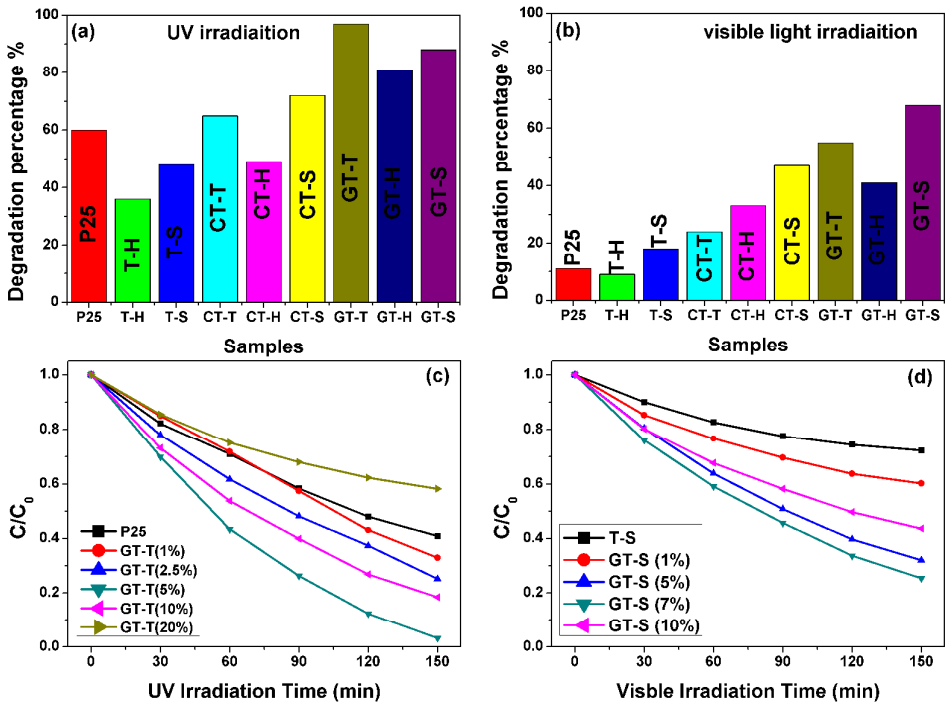

Fig 1. (a) and (b) the degradation efficiencies of Rh.B over the GT composites with 5% graphene; (c) and (d) the degradation efficiencies of Rh.B over the GT-T and GT-S with different content of graphene under UV and visible irradiation respectively.

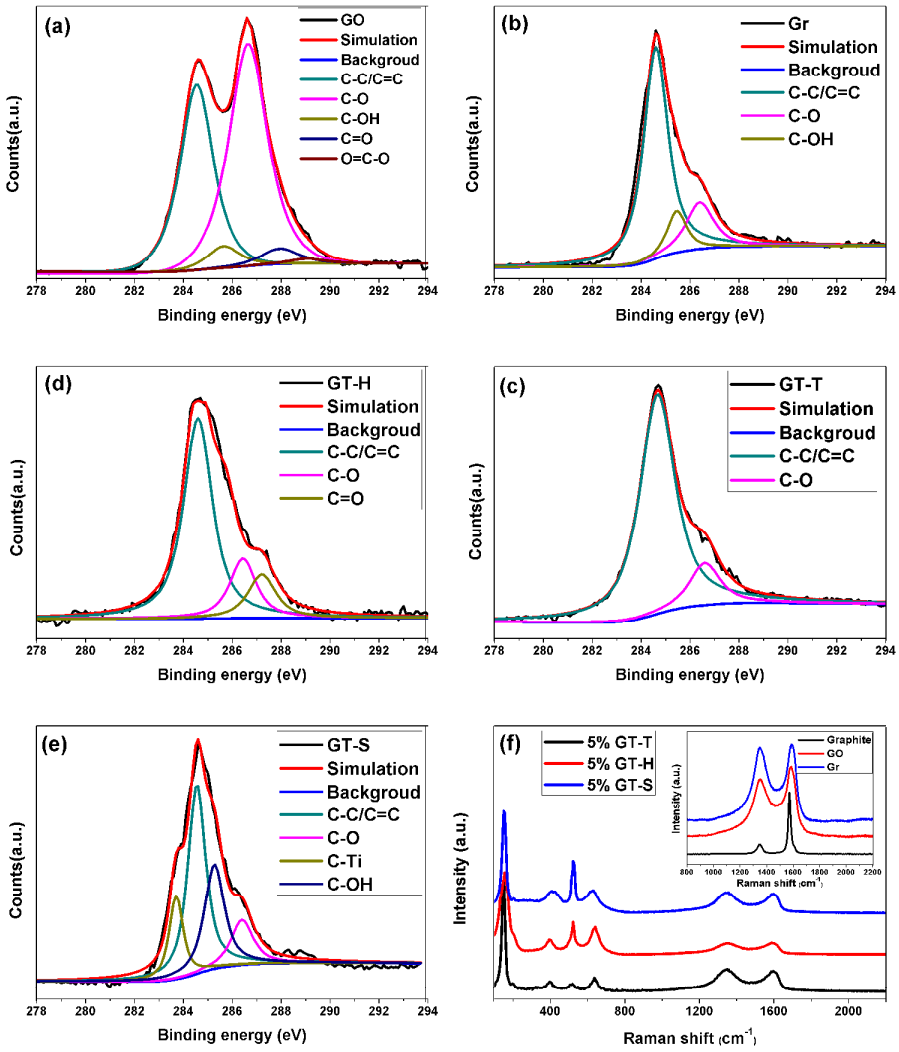

Fig. 2 (a-e) the high resolution C 1s XPS spectra for the GT composites as well as GO and Gr; (f) the Raman spectra of GT.

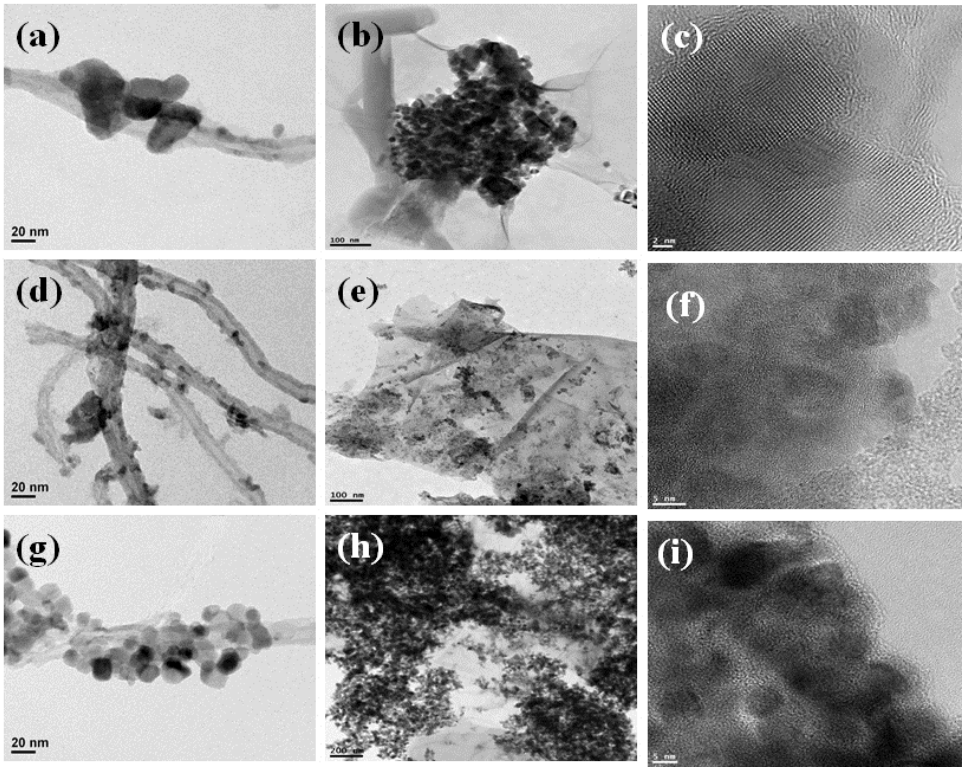

Fig. 3. The TEM images of the CT-T (a) GT-T (b), CT-H (d), GT-H(e), CT-S (g) and GT-S(h) composites; HR-TEM images of GT-T(c), GT-H(f) and GT-S(i)

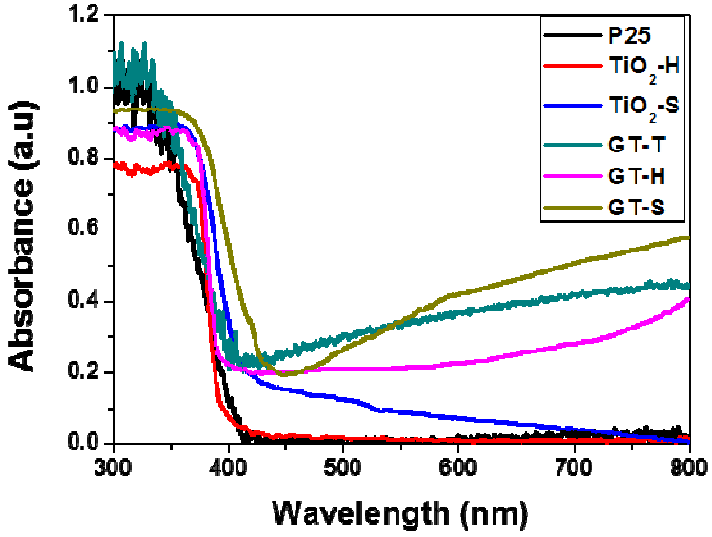

Fig. 4. Diffuse reflectance UV-vis spectroscopy of different samples.

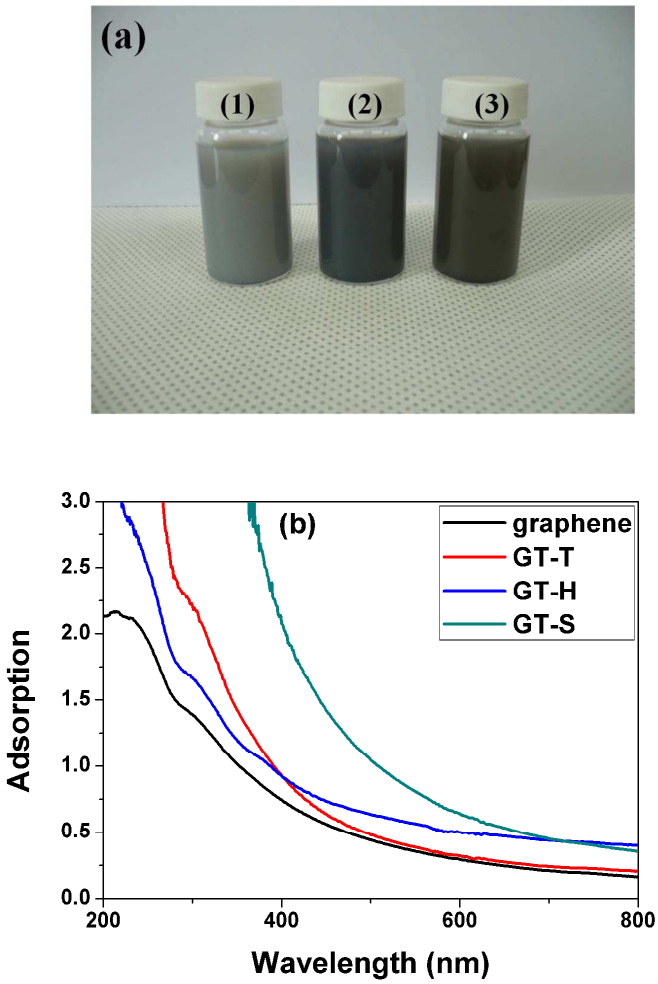

Figure 5. (a) the photographs of the GT suspensions with GT-T(1), GT-H(2) and GT-S(3); (b) UV-vis spectrum of different samples.